Wavelength agile superlattice quantum dot infrared photodetector

G. Ariyawansa,[1] A. G. U. Perera,[1,a)] G. Huang,[2] and P. Bhattacharya[2]
[1]*Department of Physics and Astronomy, Georgia State University, Atlanta, Georgia 30303, USA*
[2]*Department of Electrical Engineering and Computer Science, Solid State Electronics Laboratory, University of Michigan, Ann Arbor, Michigan 48109-2122, USA*

(Received 10 February 2009; accepted 13 March 2009; published online 3 April 2009)

A dual-band superlattice quantum dot infrared photodetector, providing bias-selectability of the response peaks, is demonstrated. The active region consists of two quantum dot superlattices separated by a graded barrier, enabling photocurrent generation only in one superlattice for a given bias polarity. Two response bands, one consisting of three peaks at 2.9, 3.2, and 4.9 μm and the other consisting of three peaks at 4.4, 7.4, and 11 μm, were observed up to 120 K for reverse and forward biases, respectively. The specific detectivity values at 80 K are 3.2 and 2.6×10^9 Jones for the 4.9 and 7.4 μm peaks. © *2009 American Institute of Physics*. [DOI: 10.1063/1.3114420]

In the field of infrared (IR) technology, quantum dot IR photodetectors (QDIPs) became attractive since the extra degree of confinement in QDs compared to quantum wells leads to low dark currents.[1] In addition, QDs allow normal incidence detection, which is the primary challenge in quantum well IR photodetectors (QWIPs). The dark current of the QD structures has been further reduced using resonant tunneling concept,[2] while the QDIPs also exhibit multicolor characteristics.[3] In general, an IR detector or a focal plane array camera[4] captures the intensity profile of the scene. However, if the information of the scene can be captured using two or more spectral bands, that would be useful to reconstruct the complete thermal profile of the scene and reduce false positives. Hence, the development of detectors with multiband characteristics and the ability to select spectral bands will immensely aid various applications including land-mine detection, missile-warning sensors, identification of muzzle flashes from firearms, and space situational awareness.[5] In addition, multiband IR detectors can also be operated as single band detectors in each of the spectral bands.

The major challenge associated with multiband detectors so far is the selection of the operating wavelength without using external optical filters or multiterminal electrical contacts on the detector. In addition to reducing the radiation transmission, external optical filters with complicated mechanical drives increase the weight of the system. Although detectors[6,7] consisting of two active regions with more than two electrical contacts allow simultaneous detection of the photosignals in the two spectral bands, the arrays made of such detectors require sophisticated fabrication techniques. To avoid these drawbacks, a tunneling-QDIP (T-QDIP) (Ref. 8) was reported, which provided dual-band detection capability with a selection of the operating wavelength by alternating the applied bias voltage polarity. This work demonstrated the idea and the feasibility of using QDIP structures for developing detectors with specific capabilities. However, this detector did not demonstrate complete wavelength selectivity, i.e., the spectral crosstalk between the two bands was not eliminated. The primary reason was a response peak associated with the transition to the QD wetting layer (WL), which could not be controlled using bias. Hence, a QD structure, a superlattice QDIP (SL-QDIP), which is capable of detecting radiation in two spectral bands with improved wavelength selection capability, was designed, grown, experimentally tested, and reported in this letter. As an additional advantage compared to the T-QDIP,[8] the SL-QDIP provides response wavelength tunability at the detector design stage without changing the QD size. Compared to the previously reported superlattice QWIP structure,[9] which showed a response at 10 K with either 45-incidence configuration or corrugated geometry, the SL-QDIP shows a similar responsivity at 80 K with normal incidence geometry. Hence, SL-QDIP demonstrates a significant improvement in the operating temperature with normal incidence detection, providing straightforward device fabrication for arrays.

A schematic diagram of the SL-QDIP structure grown by molecular beam epitaxy is shown in Fig. 1. The structure consists of two QD-SLs (labeled as top and bottom QD-SLs) separated by a graded $Al_xGa_{1-x}As$ barrier ($x=0.09-0.3$), which are sandwiched in two highly doped ($n=2\times10^{18}$ cm^{-3}) GaAs contact layers. The two QD-SLs are identical and consist of self-assembled $In_{0.4}Ga_{0.6}As$ QDs placed in a SL made of five periods of 90 Å GaAs/30 Å $Al_{0.4}Ga_{0.6}As$ quantum wells (see Fig. 1). The pyramidal shape QDs have height and base dimensions of ~6 and ~20 nm, respectively, and were *n*-doped to 1.5×10^{18} cm^{-3} using Si. The GaAs and AlGaAs layers were grown at 610 °C, while the $In_{0.4}Ga_{0.6}As$ QDs were grown at 500 °C on top of a WL with a thickness of ~3 ML. While this structure consists of one active period (top QD-SLs/graded barrier/bottom QD-SL), it is also possible to use multiple periods, which can be expected to show high performance due to the increase in light absorption. However, the number of periods has to be determined to optimize the performance, taking growth issues into account. Vertical circular mesas for top illumination were fabricated by standard photolithography, wet chemical etching, and contact metallization techniques. The highly doped *n*-type top and bottom ring contacts were formed by evaporated Ni/Ge/Au/Ti/Au with thicknesses of 250/325/650/200/2000 Å. The radius of the optically active area of a processed device was 300 μm.

A schematic band diagram showing the conduction band profile of the structure under zero bias is shown in Fig. 2(a). The bound states in QDs calculated by an eight-band $\mathbf{k}\cdot\mathbf{p}$ model[10] (E_0, E_1, and E_2) and minibands (M_1 and M_2) in both

a)Electronic mail: uperera@gsu.edu. Also at NDP Optronics, LLC.

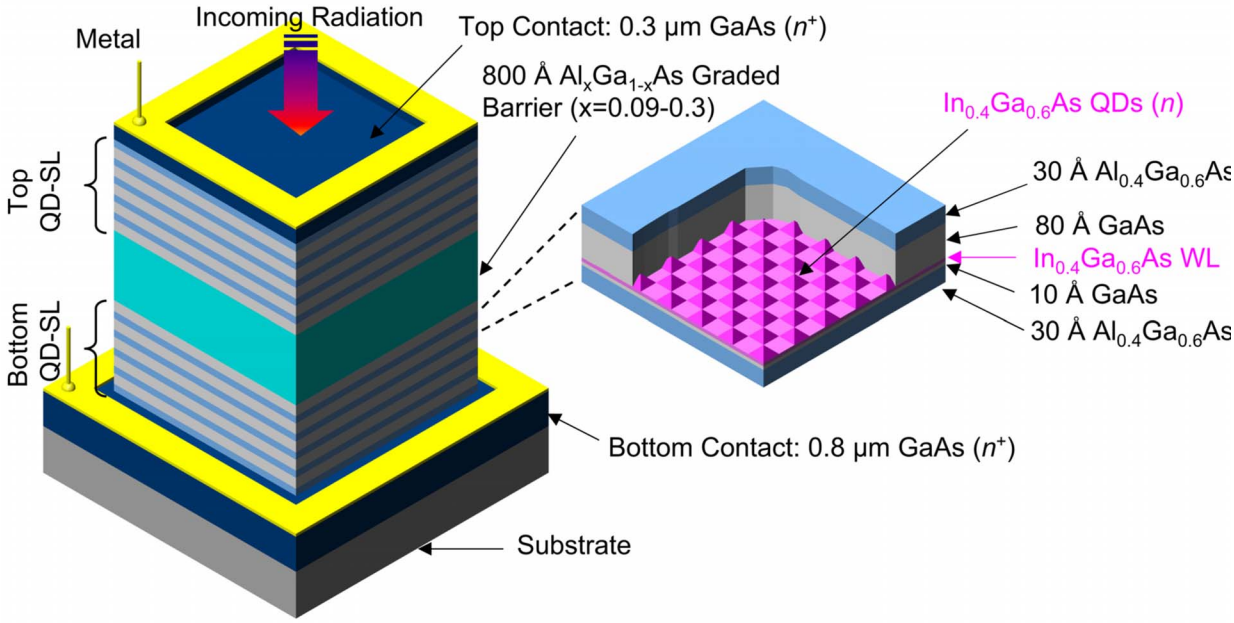

FIG. 1. (Color online) Structure of the SL-QDIP detector. Two QD-SLs (top and bottom QD-SLs) are separated by a thick linearly graded $Al_xGa_{1-x}As$ ($x=0.09-0.3$) barrier, which in turn are sandwiched between two highly doped ($n=1.5\times10^{18}$ cm^{-3}) GaAs contact layers. Each SL consists of five n-doped (1.5×10^{18} cm^{-3}) $In_{0.4}Ga_{0.6}As$ QD layers placed in $GaAs/Al_{0.4}Ga_{0.6}As$ wells, as shown in the expanded view.

SLs are also shown. The approach to calculate the minibands in the two SLs is explained elsewhere.[11] These bound states in the QDs (E_0, E_1, and E_2) are located at -0.156, -0.065, and -0.026 eV with respect to the GaAs conduction band edge. The SLs exhibit two minibands located at 0.093 and 0.269 eV with respect to the GaAs conduction band edge. In both SLs, the effect of the WL has been taken into account. As the QDs are doped and the highly doped GaAs contact layers are separated only by a thin AlGaAs layer, all the QD energy states are filled with carriers. In this structure, optical absorption takes place in the SLs, exciting carriers from all QD states (E_0, E_1, and E_2) to the minibands. Two sets of closely spaced peaks are expected due to excitations from QD states to M_1 and M_2 minibands. The excited carriers escape over the graded barrier with the support of the applied electric field and are collected at the contacts as the photocurrent. The most important fact is that only one SL becomes active for photocurrent generation under a given bias direction (forward or reverse). As shown in Fig. 2(b), under forward bias (top positive), a response resulted in three peaks at 5.1, 7.8, and 10.5 μm is expected due to electronic transitions from QD states to the lower miniband state (M_1). Similarly, under reverse bias (top negative), a response resulted in three peaks at 2.9, 3.7, and 4.2 μm is expected due to electronic transitions from QD states to the upper miniband (M_2). Under this condition, the carriers excited to the lower miniband (M_1) cannot escape the AlGaAs graded barrier and do not contribute to the photocurrent.

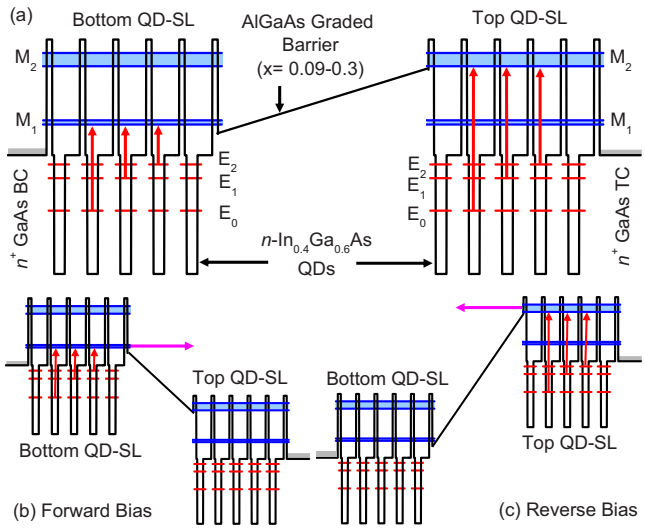

FIG. 2. (Color online) The conduction band profile of the SL-QDIP under (a) zero, (b) forward (top positive), and (c) reverse bias conditions. The bound states in QDs (E_0, E_1, and E_2) and minibands (M_1 and M_2) in both SLs are also shown. In (b) and (c), possible transitions from QD states to minibands leading to spectral response peaks are indicated by vertical arrows, while escape of carriers is indicated by horizontal arrows.

As shown in Fig. 3, the experimentally observed response peaks of the SL-QDIP at 80 and 120 K closely follow the theoretical predictions. A response with three peaks at 2.9, 3.2, and 4.9 μm with the 4.9 peak being the dominant one was observed under reverse bias. The longer wavelength threshold was observed at ~6 μm. These peaks are in good agreement with the theoretically predicted peaks at 2.9, 3.7, and 4.2 μm for reverse bias. Similarly, a response due to three peaks at 4.3, 7.4, and 11 μm with the 7.4 μm peak being the dominant one was observed under forward bias. The long wavelength threshold for this response band was observed at ~13 μm. This set of peaks is also in good agreement with the predicted peak locations (5.1, 7.8, and 10.5 μm). As in the band diagram shown in Fig. 2, a response due to the transition from the M_1 miniband to the M_2 miniband sensitive to normal incidence radiation could also be expected. However, in this structure, electron transition from M_1 is not observed since the doping is such that the Fermi level is kept below M_1, leaving the M_1 miniband empty. If the M_1-to-M_2 transition occurs, based on the calculated miniband locations (mentioned before), it should correspond to a peak around ~7 μm, and this peak should be

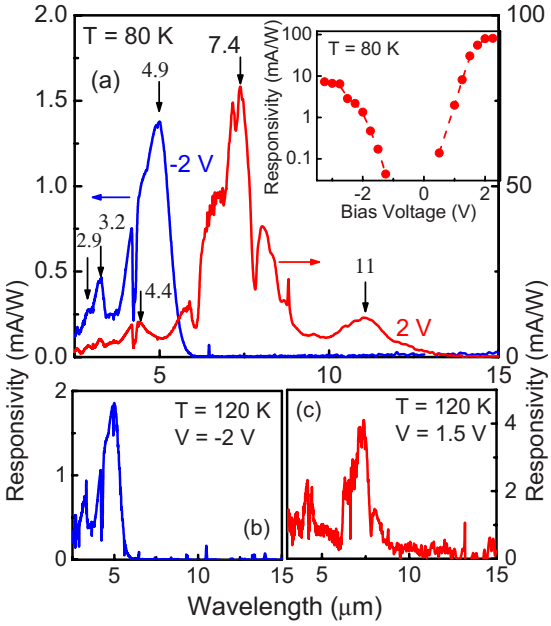

FIG. 3. (Color online) Calibrated spectral response of the SL-QDIP under forward and reverse bias conditions at 80 K. Peaks at 4.9 and 7.4 μm are observed due to transitions of electrons from QD states to the upper (for reverse bias) and lower minibands (for forward bias), respectively. Variation in the responsivity with bias voltage at 7.4 μm for forward bias and at 4.9 μm for reverse bias is shown in the inset. The response at 120 K is shown in (b) for reverse and (c) for forward bias.

dominant for forward bias. However, this was not observed for forward bias, confirming that M_1-to-M_2 transition does not take place in this structure. As an overall comment, the dominant response peaks were based on the electronic transitions from the upper QD states, implying that the transitions from upper most states are more efficient. However, for the response under forward bias, the transition from the E_3 state is weaker than that from the E_2 state. This observation could be due to incomplete carrier occupancy in the E_3 state. Moreover, the variation in the responsivity with bias voltage at 7.4 μm for forward and at 4.9 μm for reverse bias is shown in the inset of Fig. 3(a). Also, the response at 120 K for reverse and forward bias is shown in Figs. 3(b) and 3(c), respectively.

Although the two response bands in this detector are not confined purely in the 3–5 and 8–14 μm atmospheric windows as seen in Fig. 3(a), the structure can be modified to obtain responses solely in the two atmospheric windows, which would be of highly interested for practical applications. By adjusting the parameters in the bottom QD-SL, the long wavelength response can be pushed into the 8–14 μm region. In this way, the spectral overlap between the two spectral bands can be further reduced.

The experimental dark current density of the SL-QDIP at temperatures up to 200 K is shown in Fig. 4(a). The asymmetry in the dark current can be attributed to the difference in the effective barrier for the electrons in the two QD-SLs. The wavelength threshold, which corresponds to the activation energy obtained from Arrhenius model, is shown in Fig. 4(b). For low bias (~0.5 V), the wavelength threshold agrees with the theoretically predicted response, while it rapidly increases with bias. This could be due to tunneling dominant dark current as opposed to thermal at high bias. However, the threshold for forward bias is longer than that of

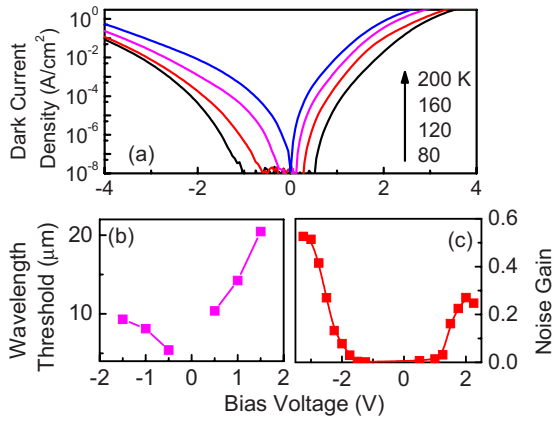

FIG. 4. (Color online) Dark current density of the SL-QDIP at temperatures between 80 and 200 K. (b) Variation in the wavelength threshold with bias calculated based on Arrhenius model. (c) Variation in the noise gain based on the measured noise current and dark current.

reverse bias, as expected. Using the measured noise current spectra, the detectivity values were obtained as 3.2×10^9 and 2.6×10^9 Jones at 80 K for the peaks at 4.9 μm (under −2 V bias) and 7.4 μm (under 2 V bias), respectively. Assuming that the photoconductive gain is similar[12] to the noise gain [see Fig. 4(c)], the quantum efficiency of the SL-QDIP was obtained to be ~0.4 and 5% at 4.9 and 7.4 μm, respectively.

In summary, a SL-QDIP exhibiting two bias-selectable response bands with peak wavelengths at 4.9 and 7.4 μm was reported. In this structure, QDs were placed in two SLs, which were separated by a graded barrier. Electronic transitions from QD bound states to the upper and lower minibands in the SLs led to the two response bands. The graded barrier incorporated between the two SLs allowed collection of photocarriers excited to the lower and upper minibands for forward and reverse biases, respectively, enabling the wavelength selectivity. This design can be further modified to obtain responses solely in the two atmospheric windows.

This work is supported in part by the U.S. Air Force under STTR Contract No. FA9550-09-C-0106 and the U.S. NSF under Contract No. ECCS-0620688. The authors acknowledge fruitful discussions with Dr. S. G. Matsik.

[1] P. Martyniuk, S. Krishna, and A. Rogalski, J. Appl. Phys. **104**, 034314 (2008).
[2] P. Bhattacharya, X. H. Su, S. Chakrabarti, G. Ariyawansa, and A. G. U. Perera, Appl. Phys. Lett. **86**, 191106 (2005).
[3] G. Ariyawansa, A. G. U. Perera, G. S. Raghavan, G. von Winckel, A. Stintz, and S. Krishna, IEEE Photonics Technol. Lett. **17**, 1064 (2005).
[4] A. Rogalski, Opto-Electron. Rev. **12**, 221 (2004).
[5] P. M. Alsing, D. A. Cardimona, D. H. Huang, T. Apostolova, W. R. Glass, and C. D. Castillo, Infrared Phys. Technol. **50**, 89 (2007).
[6] M. P. Touse, G. Karunasiri, K. R. Lantz, H. Li, and T. Mei, Appl. Phys. Lett. **86**, 093501 (2005).
[7] R. C. Jayasinghe, G. Ariyawansa, N. Dietz, A. G. U. Perera, S. G. Matsik, H. B. Yu, I. T. Ferguson, A. Bezinger, S. R. Laframboise, M. Buchanan, and H. C. Liu, Opt. Lett. **33**, 2422 (2008).
[8] G. Ariyawansa, V. Apalkov, A. G. U. Perera, S. G. Matsik, G. Huang, and P. Bhattacharya, Appl. Phys. Lett. **92**, 111104 (2008).
[9] A. Majumdar, K. K. Choi, J. L. Reno, and D. C. Tsui, Appl. Phys. Lett. **86**, 261110 (2005).
[10] H. Jiang and J. Singh, Phys. Rev. B **56**, 4696 (1997).
[11] E. Anemogiannis, E. N. Glytsis, S. Member, and T. K. Gaylord, IEEE J. Quantum Electron. **33**, 742 (1997).
[12] B. Aslan, H. C. Liu, A. Bezinger, P. J. Poole, M. Buchanan, R. Rehm, and H. Schneider, Semicond. Sci. Technol. **19**, 442 (2004).